

Nearly 30,000 late-type main-sequence stars with stellar age from LAMOST DR5

JIAJUN ZHANG,^{1,2} JINGKUN ZHAO,¹ TERRY D. OSWALT,³ XILONG LIANG,^{1,2} XIANHAO YE,^{1,2} AND GANG ZHAO^{1,2}

¹*CAS Key Laboratory of Optical Astronomy, National Astronomical Observatories, Chinese Academy of Sciences, Beijing 100101, China.*
zjk@nao.cas.cn

²*School of Astronomy and Space Science, University of Chinese Academy of Sciences, Beijing 100049, China*

³*Embry-Riddle Aeronautical University, Aerospace Boulevard, Daytona Beach FL, USA, 32114. oswaltt1@erau.edu*

Submitted to ApJ

ABSTRACT

We construct a sample of nearly 30,000 main-sequence stars with $4500\text{K} < T_{\text{eff}} < 5000\text{K}$ and stellar ages estimated by the chromospheric activity–age relation. This sample is used to determine the age distribution in the $R - Z$ plane of the Galaxy, where R is the projected Galactocentric distance in the disk midplane and Z is the height above the disk midplane. As $|Z|$ increases, the percentage of old stars becomes larger. It is known that scale-height of Galactic disk increases as R increases, which is called flare. A mild flare from $R \sim 8.0$ to 9.0 kpc in stellar age distribution is found. We also find that the velocity dispersion increases with age as confirmed by previous studies. Finally we present spiral-shaped structures in $Z - v_Z$ phase space in three stellar age bins. The spiral is clearly seen in the age bin of $[0, 1]$ Gyr, which suggests that a vertical perturbation to the disk probably took place within the last ~ 1.0 Gyr.

Keywords: Stellar activity; Stellar ages; Stellar kinematics; Late-type dwarf stars

1. INTRODUCTION

Stellar ages are very important to understanding the formation and evolution of the Milky Way (Soderblom 2010). Evolutionary isochrones are frequently used to determine age. By placing a star on model isochrones in the Hertzsprung-Russell Diagram (HRD), the age or a limit on age can be estimated by interpolation. This method is well-suited for older stars, massive stars and evolved stars. However, for young stars (ages less than $\sim 1/3$ of their overall main-sequence (MS) lifetime) and low-mass stars, it is unsuitable (Soderblom 2010).

For late-type MS stars, several empirical relations are usually used to derive ages: gyrochronology, chromospheric activity (CA) and lithium depletion (Skumanich 1972; Barnes 2007; Mamajek & Hillenbrand 2008; Soderblom 2010). Gyrochronology is a technique based on the relation between stellar rotation period and age (Barnes 2007). Stellar rotation slows due to magnetic braking as a star grows older. Barnes (2007) obtained an empirical relation between rotation period, $B - V$ color and age using open clusters and the sun whose ages are well-known. As a star grows older, the CA declines, so it can serve as an age indicator (Skumanich 1972; Soderblom et al. 1991; Mamajek & Hillenbrand 2008). Combining the cluster CA data with modern cluster age estimates, Mamajek & Hillenbrand (2008) derived a CA–age relation for F7-K2 dwarfs with typical precision of ~ 0.2 dex between ~ 0.6 -4.5 Gyr. They used the CA–age relation to estimate ages for 108 solar-type field dwarfs within 16 pc. The number of stars was small because of color ($0.5 < B - V < 0.9$), parallax, and absolute magnitude constraints.

The Large Sky Area Multi-Object Fiber Spectroscopic Telescope Data Release 5 (LAMOST DR5) has obtained more than eight million stellar spectra with a resolution of ~ 1800 at the 5500\AA (Zhao et al. 2006, 2012; Cui et al. 2012; Deng et al. 2012; Luo et al. 2015). These spectra cover the wavelengths of Ca II HK lines (3968\AA and 3934\AA) and are sufficient to measure CA (Fang et al. 2018; Zhang et al. 2019, 2020). Zhang et al. (2019) (hereafter Paper

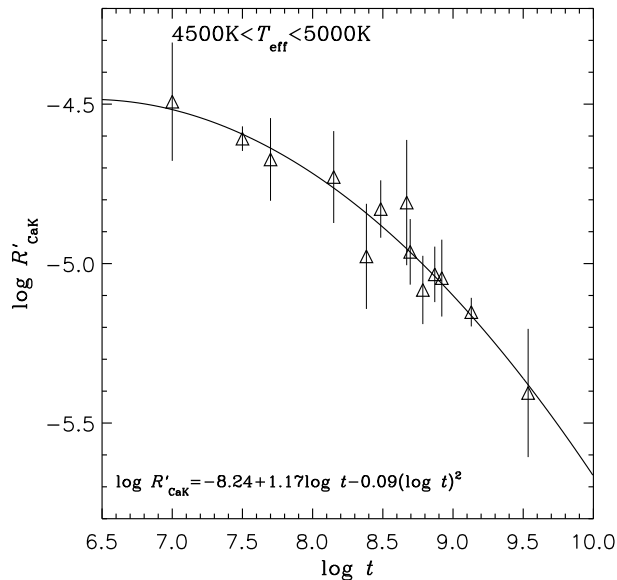


Figure 1. Relation between CA index, $\log R'_{\text{CaK}}$, and age ($\log t$) among open clusters (Details can be found in Paper I). Each triangle and error bar stands for mean value and standard deviation of $\log R'_{\text{CaK}}$, respectively, for member stars within each cluster. The abscissa is age in log form. The Figure includes stars only with $4500\text{K} < T_{\text{eff}} < 5000\text{K}$. The quadratic function fitted to these points is listed in the bottom-left corner. The solid line is the corresponding curve.

I) calculated a CA index, $\log R'_{\text{CaK}}$, for member stars of open clusters and studied the CA–age relations in different effective temperature (T_{eff}) ranges. This provides a way to roughly estimate ages for late-type MS stars in the LAMOST survey. Although the derived ages have relatively large uncertainties and could be affected by factors such as mass, binary companions, etc., it is possible to estimate ages for a large number of field stars for statistical analysis.

Many authors have studied the relation between stellar kinematics and age using red giant stars, sub-giant stars or MS turn-off stars instead of late-type MS stars, because ages are easier to estimate and they can be observed to larger distances than late-type MS stars (Xiang et al. 2017; Tian et al. 2018; Yu & Liu 2018; Mackereth et al. 2019; Wu et al. 2019). For example, Xiang et al. (2017) estimated ages for over 900,000 MS turn-off and sub-giant stars from the LAMOST Survey. They found stellar ages exhibited positive vertical and negative radial gradients across the Galactic disk. The age–velocity dispersion relation (AVR) has been studied by many authors (Wielen 1977; Nordström et al. 2004; Mackereth et al. 2019). It is well known that velocity dispersion increases with age.

Vertical phase mixing is an important phenomena in the Galactic disk (Antoja et al. 2018; Tian et al. 2018; Li & Shen 2020). It usually manifests as spiral structures of Galactocentric azimuthal velocities (v_{ϕ}) or radial velocities (v_R) in the phase space of $Z - v_Z$, where Z is the height above the disk midplane and v_Z is the velocity component perpendicular to the midplane. Tian et al. (2018) found that the spiral structures existed in populations of stars with age less than 0.5 Gyr, which supported the conclusion that the vertical perturbation took place no later than 0.5 Gyr.

Few studies have used late-type MS stars to investigate the relation between kinematics and age. Zhao et al. (2013), using CA index S_{HK} measurements for over 13,000 F, G, and K disk stars in the Sloan Digital Sky Survey (SDSS) Data Release 7 (DR7) spectroscopic sample, found the fraction of K dwarfs that had strong CA dropped with vertical distance from the Galactic midplane. Those active stars were relative young. Because of dynamical heating in the thin disk, older stars are more likely to be found farther from the Galactic plane. We used late-type MS stars with estimated ages to study kinematics. The results were then compared to other studies which used sub-giant stars or red giant stars.

This paper is organized as follows: Section 2 introduces the sample and how ages for late-type MS stars were estimated. The relation between stellar kinematics and age is discussed in section 3. Our conclusions are summarized in section 4.

2. LATE-TYPE MS STARS WITH ESTIMATED AGES

2.1. CA–age relation of stars with $4500K < T_{\text{eff}} < 5000K$ and $[Fe/H] > -0.2$

In Paper I, we calculated the CA index, $\log R'_{\text{CaK}}$, based on the Ca II K line for member stars of 82 open clusters. These stars are all FGK dwarfs. In Paper I, the CA–age relation was investigated in different T_{eff} ranges. Figure 1 displays relation between the CA index ($\log R'_{\text{CaK}}$) and age ($\log t$) for stars with $4500K < T_{\text{eff}} < 5000K$ (T_{eff} was provided by LAMOST DR5). The updated member star catalogue provided by Cantat-Gaudin & Anders (2020) was used. For M67, we used member stars provided by Carrera et al. (2019) instead of Cantat-Gaudin & Anders (2020) because catalogue of former study included more member stars. Those stars labeled as ‘Flare*’, ‘pMS*’, ‘YSO’, ‘RSCVn’, ‘SB*’, ‘EB*WUMa’, ‘EB*’, ‘EB*Algol’ and ‘EB*betLyr’ by Simbad were excluded. In Figure 1, each triangle and error bar stands for the mean value and standard deviation of $\log R'_{\text{CaK}}$, respectively, for member stars within each open cluster, while the abscissa is the age ($\log t$). Table 1 lists the relevant data for these open clusters: cluster name, logarithm of age (from HRD), age in million years, mean value of metallicity from LAMOST DR5, standard deviation in metallicity, number of stars, $\log R'_{\text{CaK}}$ index, standard deviation in $\log R'_{\text{CaK}}$, estimated age from CA and relative difference between estimated age and accurate age. We used a quadratic function to fit these data points, shown as a solid line in Figure 1 and given in Equation 1, which was used to estimate ages for late-type MS stars with $4500K < T_{\text{eff}} < 5000K$ and $[Fe/H] > -0.2$. This metallicity limit was chosen because open clusters have average $[Fe/H] > -0.2$ (see Table 1). We then estimated ages for open clusters using Equation 1 and the results were shown in Table 1. The largest deviations from the curve in Figure 1 occurred in NGC_1039, Roslund_6 and NGC_2281 (see Table 1). Note that only two clusters (NGC_752 and M67) are larger than 1.0 Gyr. Open clusters older than 1 Gyr are more difficult to observe than young clusters.

$$\log R'_{\text{CaK}} = -8.24 + 1.17 \log t - 0.09(\log t)^2, \quad 4500K < T_{\text{eff}} < 5000K \text{ and } [Fe/H] > -0.2 \quad (1)$$

Table 1. open clusters of Figure 1

Name	$\log t$	$t(\text{Myr})$	$[Fe/H]_{\text{LA}}$	$[Fe/H]_{\text{stdLA}}$	N	$\log R'_{\text{CaK}}$	$\log R'_{\text{CaK-std}}$	$t'(\text{Myr})$	Relative difference(%)
ASCC_16	7.0	10	-0.13	0.074	4	-4.49	0.186	5	-46
ASCC_19	7.5	32	-0.12	0.025	3	-4.61	0.039	38	+20
α Per	7.7	50	-0.03	0.062	13	-4.67	0.130	71	+42
Pleiades	8.15	141	-0.08	0.066	28	-4.73	0.144	112	-20
NGC_1039	8.383	242	-0.03	0.096	12	-4.98	0.165	544	+125
ASCC_23	8.485	305	-0.09	0.080	2	-4.83	0.090	226	-25
Roslund_6	8.67	468	-0.05	0.047	5	-4.81	0.196	198	-57
NGC_1662	8.695	490	-0.04	0.003	2	-4.96	0.103	503	+1
NGC_2281	8.785	603	-0.05	0.058	4	-5.08	0.107	936	+53
Hyades	8.87	741	0.07	0.119	3	-5.03	0.087	732	-1
Praesepe	8.92	832	0.13	0.064	17	-5.05	0.121	777	-6
NGC_752	9.13	1349	-0.04	0.064	5	-5.15	0.045	1306	-3
M67	9.535	3388	-0.02	0.059	7	-5.41	0.201	3866	+12

NOTE—First column is the name of the open cluster. The $\log t$ and t are age of the cluster in logarithmic and decimal format, respectively. The ages of all clusters except for Hyades come from Kharchenko et al. (2013), while the age of Hyades comes from Gossage et al. (2018). $[Fe/H]_{\text{LA}}$ and $[Fe/H]_{\text{stdLA}}$ are the mean value and standard deviation of $[Fe/H]$ calculated from the LAMOST DR5. The subscript “LA” means LAMOST DR5. N is the number of cluster member stars with $4500K < T_{\text{eff}} < 5000K$ within each cluster. The $\log R'_{\text{CaK}}$ and $\log R'_{\text{CaK-std}}$ are the mean value and standard deviation of $\log R'_{\text{CaK}}$ of each cluster, respectively. The t' is the estimated age from Equation 1. The final column is the relative difference between estimated age (t') and accurate age (t) and calculated via $(t' - t)/t$.

The error bars in Figure 1 consist of two parts. One is measurement error, the other is the inherent variance of the CA index. Stars with the same ages, masses and metallicities do not necessarily have the same CA index due to

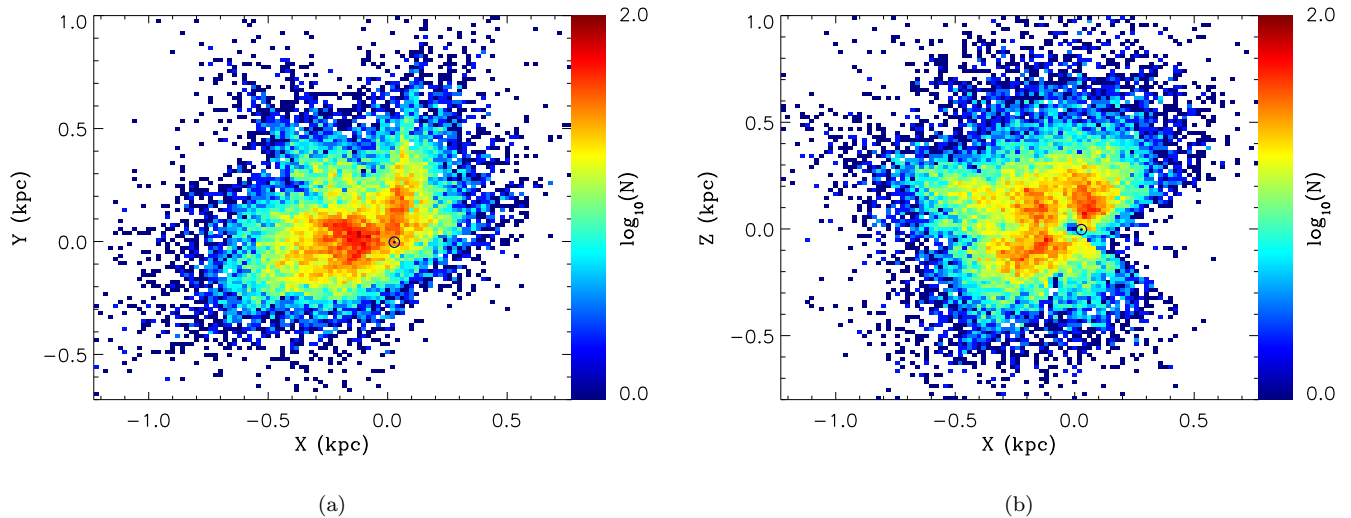


Figure 2. Colour-coded stellar spatial-density distributions in the Galactic $X - Y$ and $X - Z$ planes for late-type MS stars observed with LAMOST DR5. The dotted circle marks the location of the sun at $X = Y = Z = 0$.

different rotation rates. Because of this, an age estimate for a single star may have a large error. Here we make use of a very large sample to obtain some generalized results.

The reasons why we choose this T_{eff} range are as follows. First, at low T_{eff} the variation in the mean $\log R'_{\text{CaK}}$ with $\log t$ is larger compared to that at higher T_{eff} range. Also, there is a weak correlation between $\log R'_{\text{CaK}}$ and T_{eff} , because the R'_{CaK} value contains a contribution from the continuum, which depends on T_{eff} . Finally, the oldest open cluster, M67, has seven member stars at $4500\text{K} < T_{\text{eff}} < 5000\text{K}$ but no well observed member stars at lower T_{eff} . Narrowing the T_{eff} range to $[4500, 5000]$ K makes the CA-age relation useful to about 4.0 Gyr.

2.2. Estimating ages for late-type MS stars

By using the same method outlined in Paper I, we first calculated the CA index, $\log R'_{\text{CaK}}$, for a large number of field stars from LAMOST DR5. These field stars are the same as those in Paper I to determine the basal lines (see Section 3.2 of Paper I). The parameters of these stars are $4000\text{K} < T_{\text{eff}} < 7000\text{K}$, $\log g$ (surface gravity) > 4.0 , $-0.8 < [\text{Fe}/\text{H}] < 0.5$ and S/N_g (signal to noise ratio in g band) > 30 , provided by LAMOST DR5. The sample included 1,599,649 stars in total.

Equation 1 only applies to stars with $4500\text{K} < T_{\text{eff}} < 5000\text{K}$ and $[\text{Fe}/\text{H}] > -0.2$. And we applied these limits to the original sample. Next, we selected only stars with $-4.51 > \log R'_{\text{CaK}} > -5.41$, which corresponds to ages $0.01 < t < 4.0$ Gyr. Equation 1 was then used to estimate ages for resulting sample of 30,619 stars.

Most of these selected stars have parallaxes and proper motions provided by *Gaia* DR2 (Gaia Collaboration et al. 2018). We chose those with relative errors in parallax less than 20% and calculated heliocentric positions (X , Y and Z) relative to the sun. The X -axis points towards the Galactic center, the Y -axis points towards the Galactic rotation direction and the Z -axis points towards the Galactic north. These data are plotted in Figure 2. The LAMOST survey mainly focuses on stars in the direction of the Galactic anti-center, so there are fewer stars towards the Galactic center ($+X$) as shown in Figure 2 (Deng et al. 2012). In Figure 2(a), we see gaps in which there are fewer stars. For example, the two obvious gaps locate around $(-0.5, 0.3)$ kpc and $(-0.1, 0.5)$ kpc respectively. These gaps are caused by selection effect. The LAMOST observed stars of $-10^\circ < \delta < 60^\circ$, which excluded the region near the north celestial pole (Zhao et al. 2012). In northern summers due to weather and maintaining telescope, the observing time decreased (Zhao et al. 2012). In the following analysis, we adopted the solar Galactocentric radius and vertical positions as $(R_\odot, Z_\odot) = (8.27, 0.02)$ kpc (Schönrich et al. 2010; Schönrich 2012). Using radial velocities provided by LAMOST DR5, velocities (v_R , v_ϕ and v_Z) relative to the Galactic center were calculated. We then applied the solar motion relative to the local standard of rest (LSR), where $(U_\odot, V_\odot, W_\odot) = (8.5, 13.38, 6.49)$ km/s (Coşkunoğlu et al. 2011). The v_R is positive towards the Galactic anti-center, v_ϕ is positive towards the Galactic rotation direction and v_Z is positive

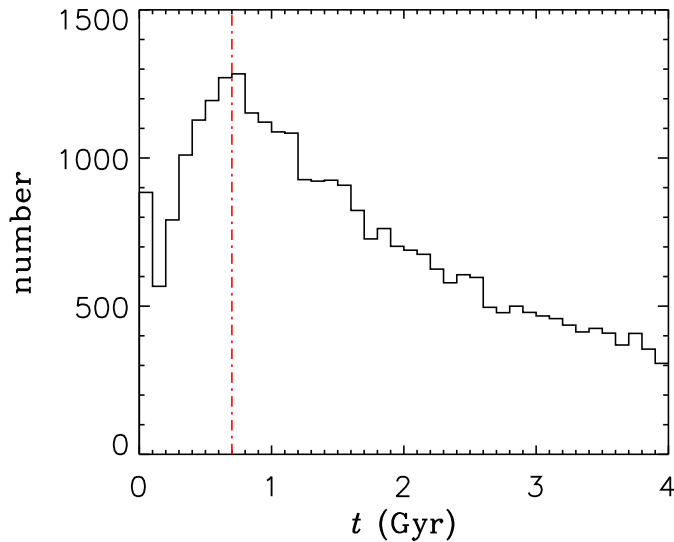


Figure 3. Age distribution of stars in our sample. The bin size is 0.1 Gyr. Dash-dot line marks the location of $t = 0.7$ Gyr.

towards the Galactic north. In total, we compiled a sample of 29,041 stars with estimated ages, space positions (X , Y and Z) and velocities (v_R , v_ϕ and v_Z).

The age distribution of this sample is shown in Figure 3. There are two peaks in this distribution: one around $t = 0.7$ Gyr and the other is the youngest bin ($t < 0.1$ Gyr). Recent studies have suggested a recent star formation burst occurred about 0.6 Gyr ago (Torres & García-Berro 2016; Davenport & Covey 2018). Ruiz-Lara et al. (2020) found three conspicuous star formation bursts occurring at 5.7, 1.9 and 1.0 Gyr ago. The star formation burst occurring at 1.0 Gyr ago is consistent with the peak of $t = 0.7$ Gyr in our age distribution within the formal uncertainty. They hypothesized that the Sagittarius dwarf galaxy pericentre passages induced the three star formation bursts. They also found a fourth possible star formation burst within the last 70 Myr, which may correspond to the peak at $t < 0.1$ Gyr in our age distribution.

3. KINEMATICS AND AGE

3.1. Age distribution in the $R - Z$ plane

Figure 4(a) displays the age distribution of our sample in the $R - Z$ plane. Here R is the projected Galactocentric distance in the disk midplane, and Z is the height above the disk midplane. Although the spatial distribution of our sample is small, we agree with the results of Xiang et al. (2017). In the vertical direction, the percentage of old stars increases as $|Z|$ increases. Thin-disk dynamical heating is believed to cause this phenomena (West et al. 2008; Casagrande et al. 2016). It is known that scale-height of Galactic disk increases as R increases, which is called flare (López-Corredoira et al. 2002). Flare is found not only via star counts, but also in stellar age distribution (Xiang et al. 2017). We can find a mild flare from $R \sim 8.0$ to 9.0 kpc in Figure 4(a). In order to further verify this flaring-age structure, we plot the median age distribution as a function of R in Figure 4(b). The sample was divided into two sub-samples with $|Z| < 0.5$ kpc and $|Z| \geq 0.5$ kpc. The expected trend that the median age decreases mildly with R can be seen, which is a characteristic of the flaring-age structure (Xiang et al. 2017; Wu et al. 2019).

3.2. Age-velocity dispersion relation

It is well known that velocity dispersion increases with age. It also correlates with orbital angular momentum L_Z , metallicity $[\text{Fe}/\text{H}]$, and height above the plane $|Z|$ (Yu & Liu 2018; Sharma et al. 2020). Our sample has $[\text{Fe}/\text{H}] > -0.2$ and distances from the Sun are less than 1 kpc. Thus, we only can consider two of these factors: age and height above the plane. We selected two sub-samples: $|Z| < 0.3$ kpc and $0.3 \text{ kpc} \leq |Z| < 0.6$ kpc. Larger $|Z|$ values could not be considered because of the small number of stars. Each sub-sample was then divided into five equal age bins between

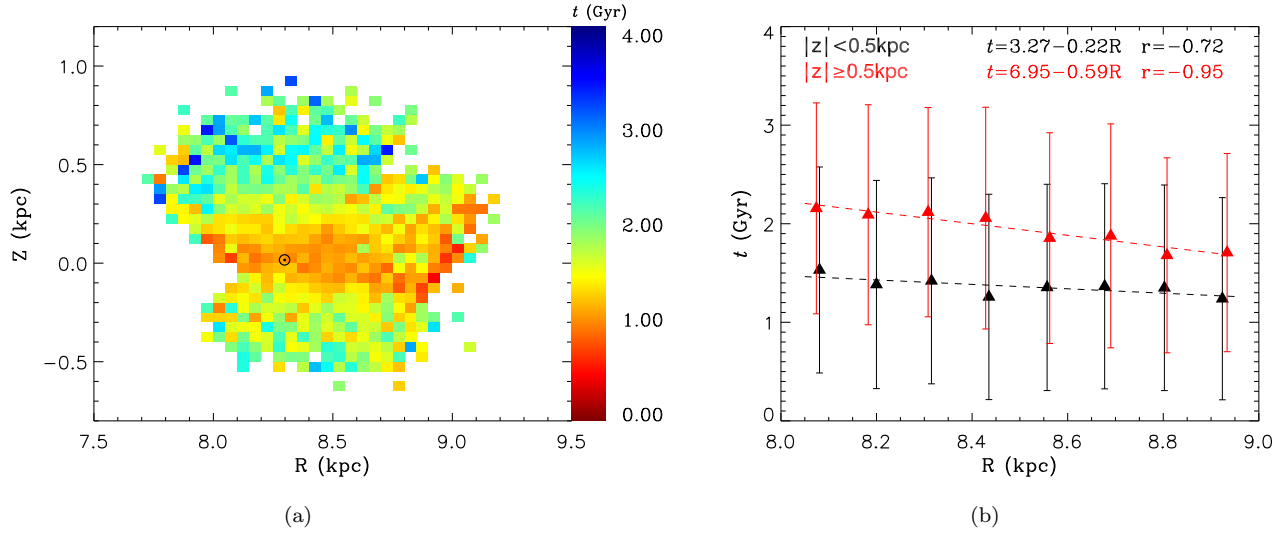


Figure 4. (a): Colour-coded distribution of the median ages of stars in the $R - Z$ plane. The adopted bin size is 0.05 kpc in both the R -direction and the Z -direction. The number of stars in each bin is larger than five. The dotted circle marks the location of the sun. (b): Median age distribution as a function of R for two sub-samples. The black triangles represent the sub-sample with $|Z| < 0.5$ kpc, while the red triangles represent the sub-sample with $|Z| \geq 0.5$ kpc. In both sub-samples, eight equal bins in $[8.0, 9.0]$ kpc are shown. The error bars represent the standard deviations of each bin's age. Linear fits for both sub-samples are indicated by the two dashed lines. The fitting relations and Pearson correlation coefficients are listed at the top.

$[0, 4.0]$ Gyr. The standard deviations of velocity components were calculated for each bin. The results are shown in Figure 5. The red trendlines and symbols represent the sub-sample with $|Z| < 0.3$ kpc, while the blue represents the sub-sample with $0.3 \text{ kpc} \leq |Z| < 0.6$ kpc. Figure 5 shows velocity dispersions increase with age, as expected from previous studies (Nordström et al. 2004; Yu & Liu 2018; Sharma et al. 2020). Thin-disk heating is believed to be the cause (Mackereth et al. 2019).

3.3. Spiral-shaped structures in $Z - v_Z$ phase space in three age bins

Antoja et al. (2018) discovered spiral-shaped structures in $Z - v_Z$ phase space, associated with vertical phase mixing of stars in the Galactic disk. It was suggested that the Galactic disk was perturbed by the Sagittarius dwarf galaxy between 300 and 900 Myr ago. In search for this pattern, we divided our sample into three stellar age bins: $[0, 1]$ Gyr, $[1, 2]$ Gyr and $[2, 4]$ Gyr. Figure 6 presents our results in the $Z - v_Z$ phase space. The color scale represents median values of v_ϕ . Hand-drawn solid line in Figure 6(a) reveals where the spiral is. The spiral is clearly seen in the youngest age bin of $[0, 1]$ Gyr, suggesting any vertical perturbation to the disk probably took place no later than 1.0 Gyr ago. Tian et al. (2018) concluded that the perturbation occurred no later than 0.5 Gyr ago. So our result and Tian et al. (2018) are roughly consistent. Figure 6 also demonstrates that as age increases, the spiral-shaped structures become less visible.

4. CONCLUSION

We re-examined the CA index $\log R'_{\text{CaK}}$ versus age $\log t$ relation for open clusters MS stars with $4500\text{K} < T_{\text{eff}} < 5000\text{K}$. Quadratic functions were fitted to obtain the relation between $\log R'_{\text{CaK}}$ and $\log t$. This relation was then applied to late-type MS stars with $4500\text{K} < T_{\text{eff}} < 5000\text{K}$ and $[\text{Fe}/\text{H}] > -0.2$ to estimate their ages. Using *Gaia* DR2 data, we removed stars with relative parallax errors larger than 20% and calculated space positions (X , Y and Z) and velocities (v_R , v_ϕ and v_Z). The final sample consisted of 29,041 late-type MS stars with estimated ages and kinematic information. Ages of stars in this sample range from 0.01 to 4.0 Gyr. Many references have used sub-giant stars or red giant stars to study the relation between stellar kinematics and age. Here, we have used late-type MS stars to investigate this relation. Our results complement and confirm their studies.

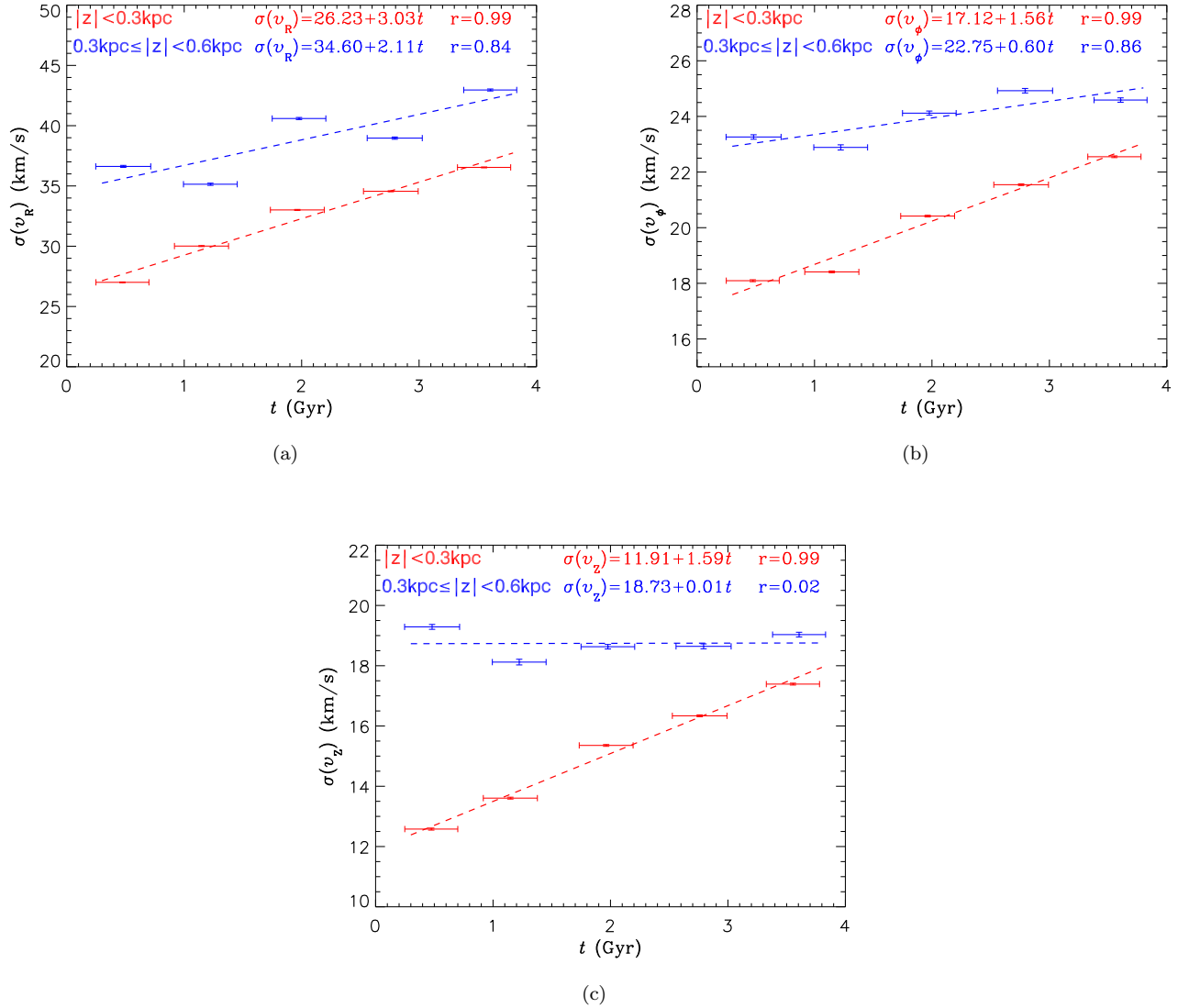


Figure 5. Velocity dispersion versus age for two sub-samples at two different $|Z|$ bins. The red symbols represent the sub-sample with $|Z| < 0.3$ kpc. The blue symbols represent the sub-sample with $0.3 \text{ kpc} \leq |Z| < 0.6$ kpc. Each sub-sample was divided into five equal age bins between $[0, 4.0]$ Gyr. The standard deviations of velocity components v_R , v_ϕ and v_z and the median values of the ages are shown. Horizontal error bars represent standard deviations for the ages. Vertical error bars were calculated via 100 Monte Carlo simulations. Dashed lines are linear least square fits. These relations and Pearson correlation coefficients are listed in the top of each panel.

Our first result is the age distribution in the $R - Z$ plane. As $|Z|$ increases, the percentage of old stars increases. We also found a mild flare in stellar age distribution along the radial direction from $R \sim 8.0$ to 9.0 kpc.

Second, the age–velocity dispersion relation was investigated. Two sub-samples were selected: $|Z| < 0.3$ kpc and $0.3 \text{ kpc} \leq |Z| < 0.6$ kpc. The expected velocity dispersion increases with age was clearly detected.

Finally, the kinematics of our sample in $Z - v_z$ phase space was investigated by dividing it into three stellar age bins: $[0, 1]$ Gyr, $[1, 2]$ Gyr and $[2, 4]$ Gyr. A spiral-shaped structure was clearly seen in the youngest age bin. This suggests that a vertical perturbation to the disk probably took place no later than 1.0 Gyr ago. As age increases, the spiral-shaped structures were shown to fade.

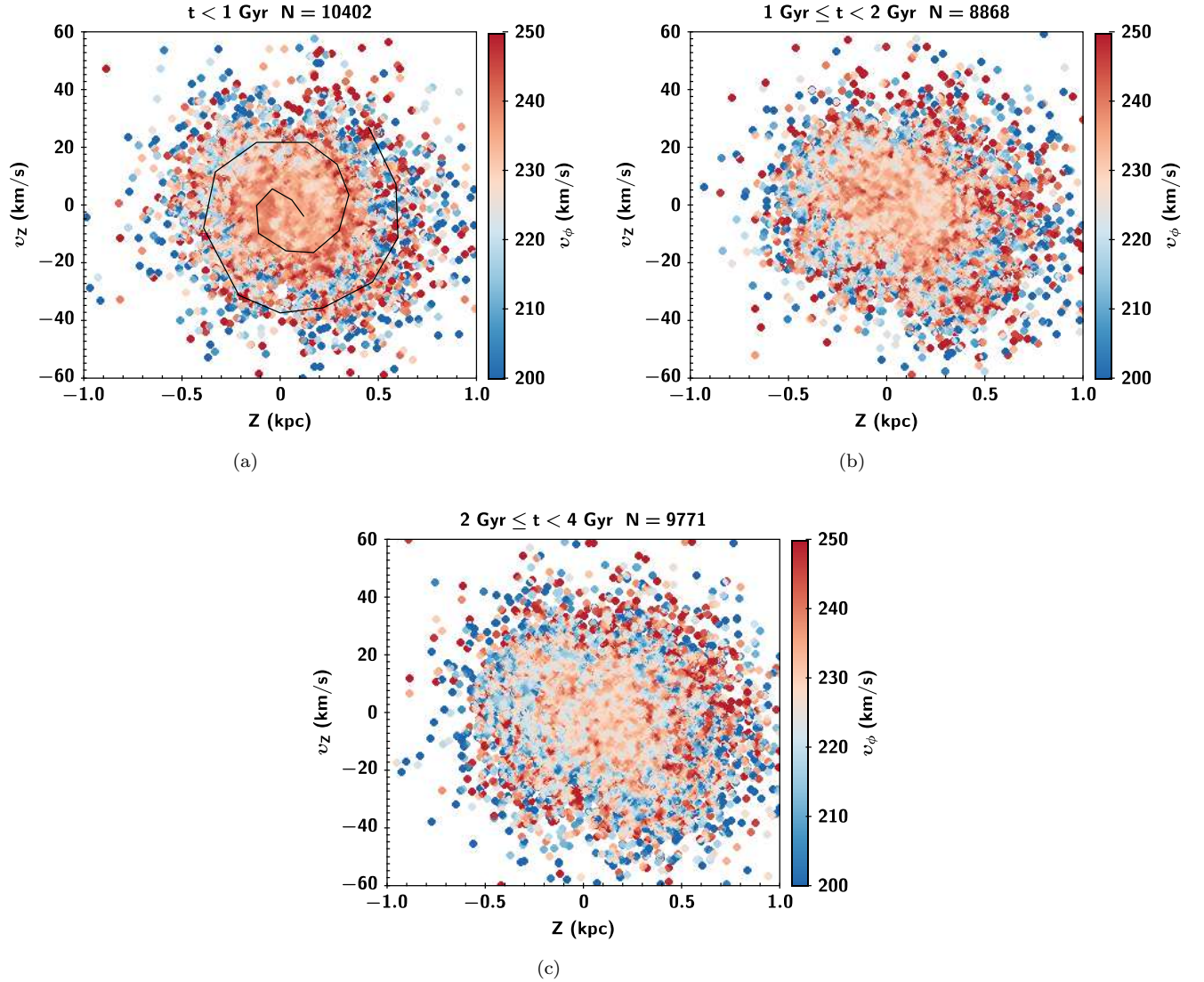


Figure 6. Search for spiral-shaped structures in the phase space of the vertical position and velocity ($Z - v_z$) for three stellar age bins: $[0, 1]$ Gyr, $[1, 2]$ Gyr and $[2, 4]$ Gyr. The color represents median value of v_ϕ . The hand-drawn solid line in (a) reveals where the spiral is. The age range and the number of stars at this age range are marked on the top of each panel.

This study is supported by the National Natural Science Foundation of China under grant No.11988101, 11973048, 11573035, 11625313, 11890694. This work is also supported by the Astronomical Big Data Joint Research Center, co-founded by the National Astronomical Observatories, Chinese Academy of Sciences and the Alibaba Cloud. Support from the US National Science Foundation (AST-1358787 and AST-1910396) to Embry-Riddle Aeronautical University is also acknowledged.

Guoshoujing Telescope (the Large Sky Area Multi-Object Fiber Spectroscopic Telescope LAMOST) is a National Major Scientific Project built by the Chinese Academy of Sciences. Funding for the project has been provided by the National Development and Reform Commission. LAMOST is operated and managed by the National Astronomical Observatories, Chinese Academy of Sciences.

This work uses data from the European Space Agency (ESA) mission Gaia (<http://www.cosmos.esa.int/gaia>), processed by the Gaia Data Processing and Analysis Consortium (DPAC, <http://www.cosmos.esa.int/web/gaia/dpac/>

consortium). Funding for the DPAC has been provided by national institutions, in particular the institutions participating in the Gaia Multilateral Agreement.

REFERENCES

- Antoja, T., Helmi, A., Romero-Gómez, M., et al. 2018, *Nature*, 561, 360
- Barnes, S. A. 2007, *ApJ*, 669, 1167
- Cantat-Gaudin, T. & Anders, F. 2020, *A&A*, 633, A99
- Carrera, R., Pasquato, M., Vallenari, A., et al. 2019, *A&A*, 627, A119
- Casagrande, L., Silva Aguirre, V., Schlesinger, K. J., et al. 2016, *MNRAS*, 455, 987
- Coşkunoğlu, B., Ak, S., Bilir, S., et al. 2011, *MNRAS*, 412, 1237
- Cui, X.-Q., Zhao, Y.-H., Chu, Y.-Q., et al. 2012, *Research in Astronomy and Astrophysics*, 12, 1197
- Davenport, J. R. A. & Covey, K. R. 2018, *ApJ*, 868, 151
- Deng, L.-C., Newberg, H. J., Liu, C., et al. 2012, *Research in Astronomy and Astrophysics*, 12, 735
- Fang, X.-S., Zhao, G., Zhao, J.-K., & Bharat Kumar, Y. 2018, *MNRAS*, 476, 908
- Gaia Collaboration, A.G.A.Brown, A.Vallenari, et al. 2018, *A&A*, 616, A1
- Gossage, S., Conroy, C., Dotter, A., et al. 2018, *ApJ*, 863, 67
- Kharchenko, N. V., Piskunov, A. E., Schilbach, E., Röser, S., & Scholz, R.-D. 2013, *A&A*, 558, A53
- Li, Z.-Y., & Shen, J. 2020, *ApJ*, 890, 85
- López-Corredoira, M., Cabrera-Lavers, A., Garzón, F., et al. 2002, *A&A*, 394, 883. doi:10.1051/0004-6361:20021175
- Luo, A.-L., Zhao, Y.-H., Zhao, G., et al. 2015, *Research in Astronomy and Astrophysics*, 15, 1095
- Mackereth, J. T., Bovy, J., Leung, H. W., et al. 2019, *MNRAS*, 489, 176
- Mamajek, E. E., & Hillenbrand, L. A. 2008, *ApJ*, 687, 1264
- Nordström, B., Mayor, M., Andersen, J., et al. 2004, *A&A*, 418, 989
- Ruiz-Lara, T., Gallart, C., Bernard, E. J., et al. 2020, *Nature Astronomy*, doi:10.1038/s41550-020-1097-0
- Schönrich, R. 2012, *MNRAS*, 427, 274
- Schönrich, R., Binney, J., & Dehnen, W. 2010, *MNRAS*, 403, 1829
- Sharma, S., Hayden, M. R., Bland-Hawthorn, J., et al. 2020, arXiv e-prints, arXiv:2004.06556
- Skumanich, A. 1972, *ApJ*, 171, 565
- Soderblom, D. R. 2010, *ARA&A*, 48, 581
- Soderblom, D. R., Duncan, D. K., & Johnson, D. R. H. 1991, *ApJ*, 375, 722
- Tian, H.-J., Liu, C., Wu, Y., et al. 2018, *ApJL*, 865, L19
- Torres, S. & García-Berro, E. 2016, *A&A*, 588, A35
- West, A. A., Hawley, S. L., Bochanski, J. J., et al. 2008, *AJ*, 135, 785
- Wielen, R. 1977, *A&A*, 60, 263
- Wu Yaqian, Xiang Maosheng, Zhao Gang, et al. 2019, *MNRAS*, 484, 5315
- Xiang Maosheng, Liu Xiaowei, Shi Jianrong, et al. 2017, *ApJS*, 232, 2
- Yu, J., & Liu, C. 2018, *MNRAS*, 475, 1093
- Zhang, J., Bi, S., Li, Y., et al. 2020, *ApJS*, 247, 9
- Zhang, J., Zhao, J., Oswalt, T. D., et al. 2019, *ApJ*, 887, 84
- Zhao, G., Zhao, Y.-H., Chu, Y.-Q., Jing, Y.-P., & Deng, L.-C. 2012, *Research in Astronomy and Astrophysics*, 12, 723
- Zhao, G., Chen, Y.-Q., Shi, J.-R., et al. 2006, *ChJA&A*, 6, 265
- Zhao, J. K., Oswalt, T. D., Zhao, G., et al. 2013, *AJ*, 145, 140